International Journal of Microwave and Wireless Technologies

cambridge.org/mrf

Dual-band transmissive linear to circular polarization converter with angular-stable and orthogonal polarizations

Bianmei Zhang[1], Chen Wang[1], Shuo Yu[1], Xiaofan Yang[2], Zhibin Fang[3] and Xiaoming Liu[1,3,4]

[1]School of Physics and Electronic Information, Anhui Normal University, Wuhu, China; [2]The State Key Laboratory of Complex Electromagnetic Environment Effects on Electronic and Information System, Luoyang, China; [3]Wuhu CEPREI Information Industry Technology Research Institute, Wuhu, China and [4]Anhui Provincial Engineering Laboratory on Information Fusion and Control of Intelligent Robot, Wuhu, China

Research Paper

Cite this article: Zhang B, Wang C, Yu S, Yang X, Fang Z, Liu X (2024) Dual-band transmissive linear to circular polarization converter with angular-stable and orthogonal polarizations. *International Journal of Microwave and Wireless Technologies* **16**(3), 515–523. https://doi.org/10.1017/S1759078723001460

Received: 14 May 2023
Revised: 15 November 2023
Accepted: 21 November 2023

Keywords:
angular stability; dual-band; orthogonal polarizations; polarization conversion

Corresponding author: Xiaoming Liu;
Email: xiaoming.liu@ahnu.edu.cn

Abstract

A dual-band angular-stable transmissive linear to circular polarization converter based on metasurface is proposed and demonstrated in this work. The converter consists of three layers. The top and bottom layers are formed by an array of double split-ring layers. The unit cell of the central layer contains a square loop nesting a slant dipole. The split-rings create two resonances, enabling dual-band operation. The slant dipole and square loop are useful for improving the quality of circular polarization conversion. It is shown that the proposed polarization converter converts the incident linearly polarized wave into circularly polarized wave with opposite polarization modes over the frequency ranges of 8.77–10.58 and 17.59–19.88 GHz. The angular stability is up to 60° for 3 dB axial ratio. Moreover, the thickness of unit cell has a wavelength below 0.06 at the lower band. Compared with other designs in the literature, the structure bears merits of wideband response, high angular stability, and low-profile property within dual-band operational region. To validate the design, a sample prototype was designed, fabricated, and measured. The measured results are in good agreement with the simulated ones.

Introduction

Polarization is one of the most important properties of electromagnetic (EM) waves [1, 2], which has seen many applications in areas such as communications and remote sensing [3, 4]. It is usually a need to effectively manipulate the polarization states of EM waves [5, 6]. Traditional methods include birefringence wave plates [7, 8] and liquid crystals [9, 10]. However, devices based on these methods have bulky configurations, making them difficult to integrate into the miniaturized system. In recent years, metasurfaces are intensively investigated as polarization converter, due to their planar nature and easy fabrication and integration [11–16].

Two types of metasurface-based polarization converter can be categorized, i.e. reflection type [17–21] and transmission type [22–33]. The reflection type bears merits of broadband operation. However, the reflection type usually blocks the emergence beam when working in normal incidence. Therefore, offset feeding is usually used. Polarization converters operating in transmission mode provide one with normal incidence and are preferential in beam steering case. They have attracted considerable attention and investigation in the literature. For the transmission type, the multilayer structures were generally applied to obtain broadband performance. In Ref. [22], a multilayer linear to circular polarization converter was proposed by inserting slot-line structures, providing with the bandwidth less than 45%. Another design [23] based on metal strips was used to achieve wideband response. However, these designs were less preferred in view of fabrication because of their size and complexity. Except for the aforementioned single-band linear to circular polarization converters, dual-band linear to circular polarization converters have been increasingly concerned for dual-band and compact communication systems [25–33]. Particularly, the polarization converters with orthogonal handedness and broadband response are much desired in dual-channel communication. However, compared with single-band linear to circular polarization converters, the dual-band linear to circular polarization converters generally suffer from narrow operation bands and low angular stabilities. In addition, the mutual effects of dual-band components make it more difficult to design [27, 29].

For example, the transmissive linear to circular polarization converter was used to realize dual-band operation with anti-polarization [25, 26]. However, the bandwidth was very narrow

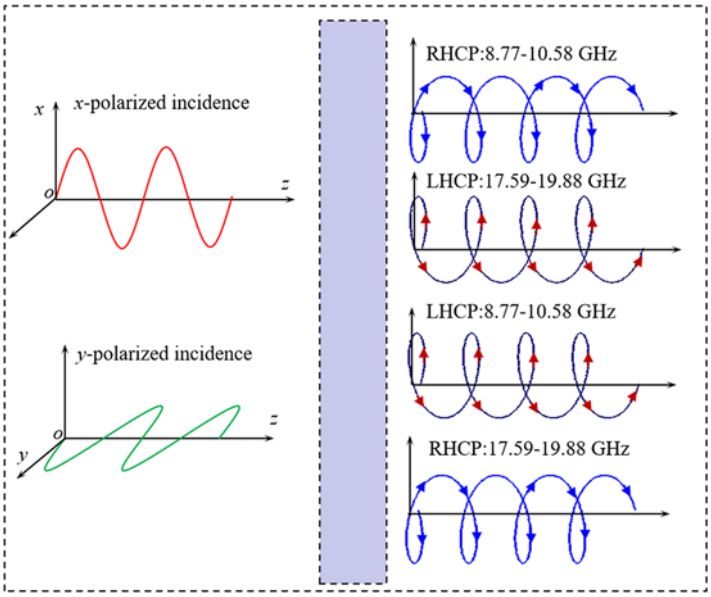

Figure 1. The working principle of linear to circular polarization converter in transmission mode.

for both designs, being less than 7%. A dual-band polarization converter based on Jerusalem cross "I"-type strip was studied [27], where the bandwidth was improved to 29%. However, the multilayer structure can be further simplified. Another design [28] was developed using single substrate, while this design only operated at x-polarized normal incidence, and performed high insertion loss due to the strong mutual interferences within dual-band operations.

Further efforts were made to increase the bandwidth and the angular stability. The dual-band polarization converter operating at K/Ka bands was introduced in Ref. [29], which can provide 20° angular stability. Similarly, a four-layer structure [30] was reported with 30° angular stability. Another two designs based on dual-layer substrates were presented in Refs [31, 32]. The angular stability reached up to 55°. However, these structures are subject to the narrow dual-band operation. In Ref. [33], a very broadband design was developed using frequency selective surfaces, providing 32% bandwidth for the first band, but the angular stability was less than 25°. It is seen that there is still much space to achieve a high-performance transmission type circular polarization converter with broadband, angular stability.

In this work, a dual-band angular-stable transmissive linear to circular polarization converter based on anisotropic metasurface is presented, as shown in Fig. 1. The structure can transform the x-polarized incident wave into right-hand circular polarization (RHCP) at lower band and left-hand circular polarization (LHCP) at higher band. It will be shown that the axial ratio (AR) of output wave remains below 3 dB in the ranges of 8.77–10.58 and 17.59–19.88 GHz, corresponding to the relatively bandwidth up to 18.71% and 12.22%, respectively. Moreover, this result is also valid for y-polarized incidence but with orthogonal polarization modes at each band. To validate the feasibility of this design, a prototype is fabricated and measured. The measured results demonstrate good agreement with the simulated ones. Compared with other polarization converters, this structure exhibits the unique advantages of low-profile, easy fabrication, high angular stability, and broadband response. In particular, the angular stability is up to 60° for 3 dB AR. Potential applications can be envisaged in a dual-band wide-angle communication system.

Principle of polarization conversion

For an incident electric field $\vec{E}^i$, it can always be decomposed into its horizontal ($\vec{E}_x^i$) and vertical ($\vec{E}_y^i$) components. Due to the anisotropic character of metasurface structure, when a linearly polarized incident wave is propagating along the $+z$ direction through the polarization converter, the $\vec{E}_x^i$ and $\vec{E}_y^i$ components will experience the different phase shifts. In most cases, the transmitted wave is seen as composed of its cross-polarization and co-polarization components. Therefore, the relationship between the incident wave and transmitted wave could be described by Jones matrix T and be written as follows [28]:

$$\begin{bmatrix} \vec{E}_x^t \\ \vec{E}_y^t \end{bmatrix} = \begin{bmatrix} t_{xx} & t_{xy} \\ t_{yx} & t_{yy} \end{bmatrix} \begin{bmatrix} \vec{E}_x^i \\ \vec{E}_y^i \end{bmatrix} = T \begin{bmatrix} \vec{E}_x^i \\ \vec{E}_y^i \end{bmatrix} \tag{1}$$

wherein $t_{xx} = |t_{xx}| e^{j\varphi_{xx}}$ and $t_{yy} = |t_{yy}| e^{j\varphi_{yy}}$ represent the co-polarization transmission, $t_{yx} = |t_{yx}| e^{j\varphi_{yx}}$ and $t_{xy} = |t_{xy}| e^{j\varphi_{xy}}$ represent the cross-polarization transmission for the incidence along x- and y-direction, respectively. In addition, the modulus sign indicates the amplitude, and φ is the phase.

Suppose an x-polarized wave is incident on the polarization converter, the amplitude and phase of the transmitted wave meets the following condition [27]:

$$|t_{xx}| = |t_{yx}|, \Delta\varphi_{xy} = \varphi_{xx} - \varphi_{yx} = 2k\pi + \frac{\pi}{2} \tag{2}$$

where k is an integer. The circularly polarized wave can be formed. Since the transmitted wave is not an ideal circular polarization wave in most cases, the AR is introduced to assess the polarization conversion properties, which can be expressed as follows [25]:

$$\begin{cases} AR = \left(\dfrac{|t_{xi}|^2 + |t_{yi}|^2 + \sqrt{a}}{|t_{xi}|^2 + |t_{yi}|^2 - \sqrt{a}} \right)^{1/2} \\ a = |t_{xi}|^4 + |t_{yi}|^4 + 2|t_{xi}|^2 |t_{yi}|^2 \cos\left(2\Delta\varphi_{xy}\right) \end{cases}, (i = x, y) \tag{3}$$

In general, the transmitted wave can be regarded as a circular polarization when its AR is lower than 3 dB. Further, to evaluate the handedness of the transmitted wave, ellipticity (e) could be

https://doi.org/10.1017/S1759078723001460 Published online by Cambridge University Press

calculated using the following equation [3]:

$$e = \sin \frac{2\,|t_{xx}| \cdot |t_{yx}| \sin \Delta\varphi_{xy}}{|t_{xx}|^2 + |t_{yx}|^2} \quad (4)$$

where ellipticity (e) value ranges from +1 to −1. The transmitted wave is an RHCP when $e = +1$ and LHCP when $e = -1$. In same way, the condition for y-polarized incidence can be also deduced.

Simulation and analysis

To design a dual-band linear to circular polarization converter with high angular stability, the schematic illustration of the unit cell of the proposed polarization converter is shown in Fig. 2. It consists of three metallic layers and two dielectric layers, where the three metallic pattern layers are separated by the dielectric substrate with height h= 1 mm, ε_r = 2.65 and tan δ = 0.001. As shown in Fig. 2(a), the metallic patterns of unit cell of the first and third layers are exactly same, and consist of two split rings, making them create dual-band operation. While the middle layer is composed of a square loop nesting a slant dipole in Fig. 2(b), which is useful for improving the performance of circular polarization conversion. Parametric sweeping is used to arrive at a satisfactory design. The sweeping goals were set to be $|t_{xx}| = |t_{yx}|$ near the frequencies of 9.5 and 18.5 GHz with a ±1 dB error. After parametric sweeping, the geometrical parameters of the unit cell are given as follows: p= 8.3 mm, g_1 = 1.88 mm, g_2 = 2.23 mm, d_1 = 0.42 mm, d_2 = 0.38 mm, l_0 = 6.8 mm, l_1 = 5.69 mm, l_2 = 3.82 mm, l_3 = 3.17 mm, and w= 0.95 mm.

The structure is modeled and simulated in Ansoft HSS using periodical boundary condition in the x-y plane and open boundary in the z-direction. The simulated results of reflection and transmission under x-polarized normal incidence are shown in Fig. 3, where $r_{ij} = |r_{ij}|\,e^{j\varphi_{ij}}$ ($t_{ij} = |t_{ij}|\,e^{j\varphi_{ij}}$) denotes i-polarized reflection (transmission) coefficients from j-polarized incidence. It can be clearly seen from Fig. 3 that the amplitudes of t_{xx} and t_{yx} are approximately equal in the frequency ranges of 8.77–10.58 GHz and 17.59–19.88 GHz. Examining the reflection coefficients, it is interesting to find that the amplitudes of r_{xx} and r_{yx} are below −9 dB in the two frequency regions. Such a result indicates that most of the incident energy penetrates through the structure with high transmission efficiency.

In addition, the phase of the two orthogonal transmission components is also shown in Fig. 4. It is seen that the phase difference of t_{xx} and t_{yx} is about −270° in the region of 8.77–10.58 GHz and +270° or −90° in the range of 17.59–19.88 GHz. Undoubtedly, the amplitude and phase criterion of circular polarization conversion

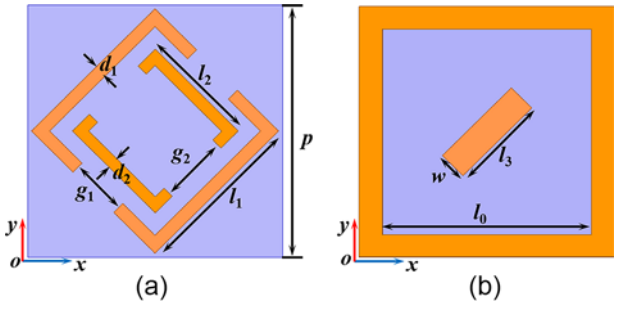

Figure 2. Schematic illustration of the unit cell for (a) the first/third layer, and (b) the second layer.

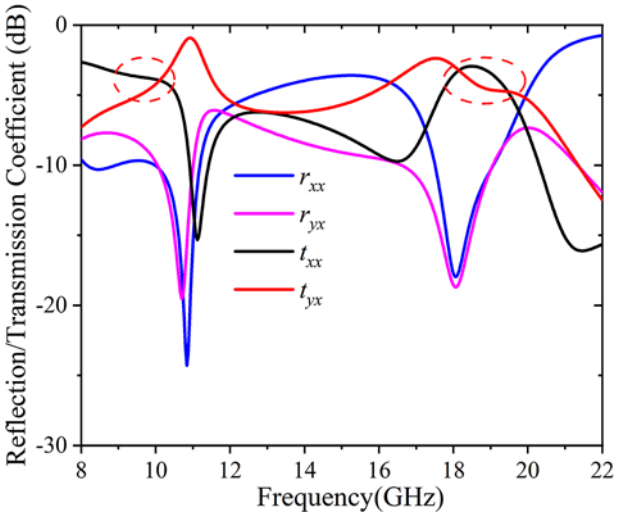

Figure 3. Reflection and transmission coefficient for x-polarized normal incidence.

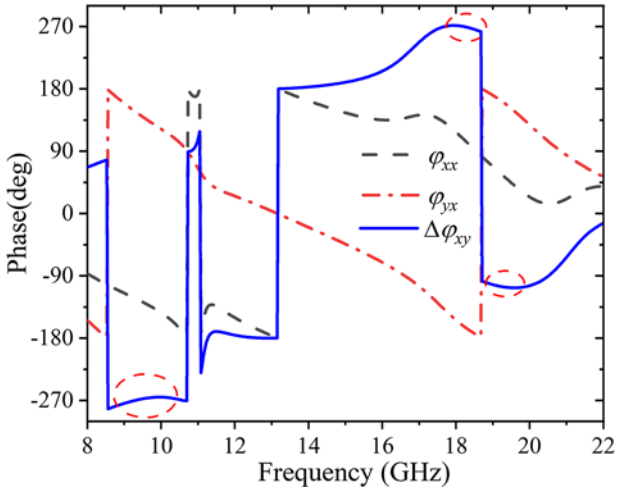

Figure 4. The phase of transmission coefficient t_{xx} and t_{yx}.

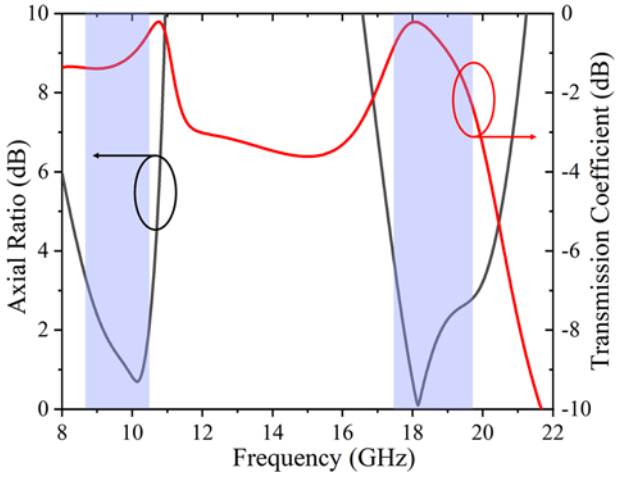

Figure 5. Simulation results of AR and transmission coefficient under normal incidence.

https://doi.org/10.1017/S1759078723001460 Published online by Cambridge University Press

are satisfied, indicating that circular polarization can be generated over the two frequency bands.

The total AR and transmission response from transmitted wave are plotted in Fig. 5. It can be observed that the AR remains below 3 dB in the ranges of 8.77–10.58 and 17.59–19.88 GHz, corresponding to the relative bandwidth of 18.71% and 12.2%, respectively. Besides, the minimum AR can be as low as 0.70 dB, indicating that a nearly perfect circularly polarized wave has been realized over two operational bands. Meanwhile, the insertion loss at two bands is less than 1.37 and 2.9 dB, and the lowest insertion loss appears in 10.59 and 18.12 GHz with value of 0.33 and 0.22 dB. Apparently, the structure can exhibit lower insertion loss at lower band. This may be attributed to the reduction of reflection coefficient and not by a particular higher depolarization effect of the unit cell, as shown in Fig. 3.

To clarify the role of each subsection of the unit cell, the evolution of the unit cell is presented in Fig. 6(a–c), which illustrate the calculated AR and ellipticity. It can be seen intuitively from Fig. 6(b) that the split-rings can transform the x-polarized incident wave into a circularly polarized wave, and create two resonances, enabling dual-band operation, where the inner and outer split-rings of unit cell have an important impact on lower and higher frequency resonances, respectively. Examining the ellipticity in Fig. 6(c), it is interesting to find that the value of ellipticity is nearly

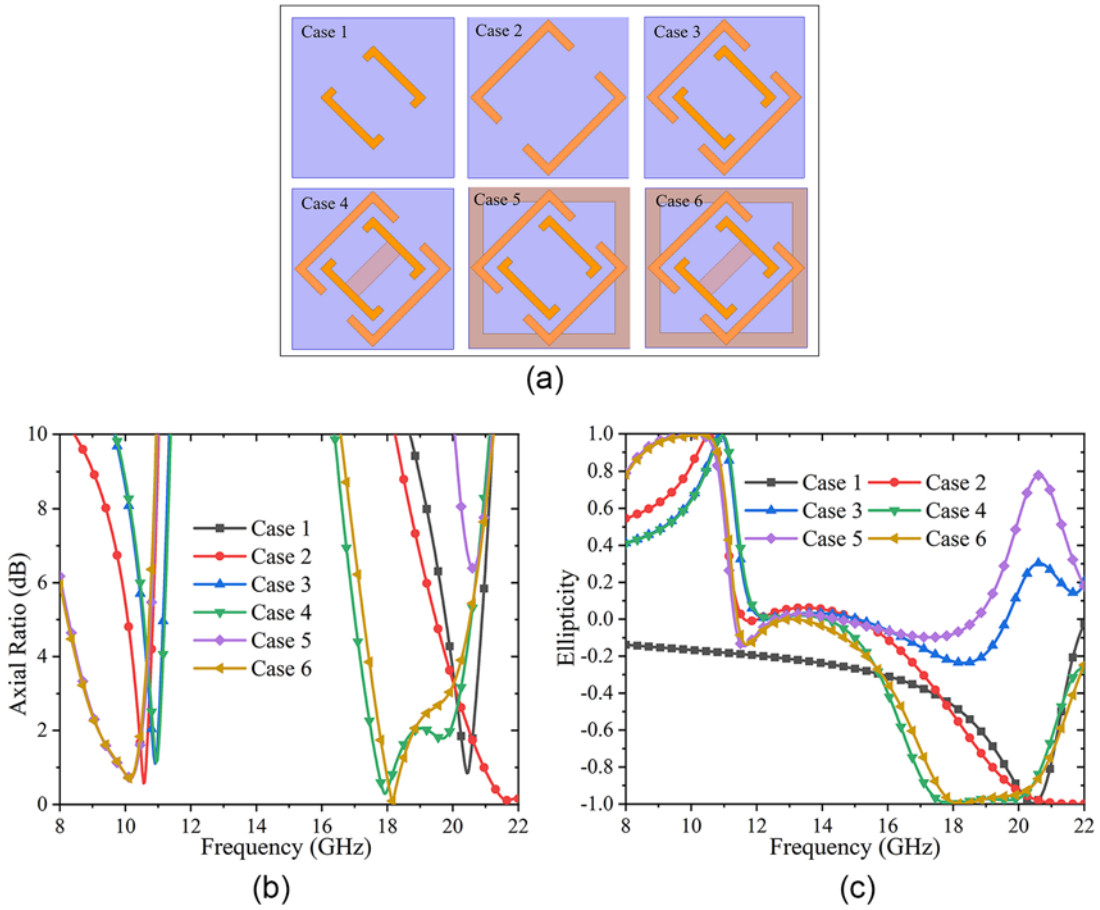

Figure 6. Simulation results of the proposed converter for (a) different configuration of the unit cell, (b) axial ratio, and (c) ellipticity.

Table 1. Performance comparison from different parts of the unit cell

Features evolution	AR (dB)	Operating band (GHz)	Operating bandwidth (GHz)	Relative bandwidth (%)	Ellipticity	Orthogonal polarization modes
Case 1	≤3	20.11–20.71	0.6	2.94	−1	No
Case 2	≤3	10.35–10.73/ 20.11–22.91	0.38/0.8	3.61/3.9	+1/−1	Yes
Case 3	≤3	10.73–11.05	0.32	2.94	+1	No
Case 4	≤3	10.77–11.08/ 17.31–20.22	0.31/2.91	2.84/15.51	+1/−1	Yes
Case 5	≤3	8.81–10.63	1.82	18.72	+1	No
Case 6	≤3	8.77–10.58/ 17.58–19.88	1.81/2.29	18.71/12.22	+1/−1	Yes

https://doi.org/10.1017/S1759078723001460 Published online by Cambridge University Press

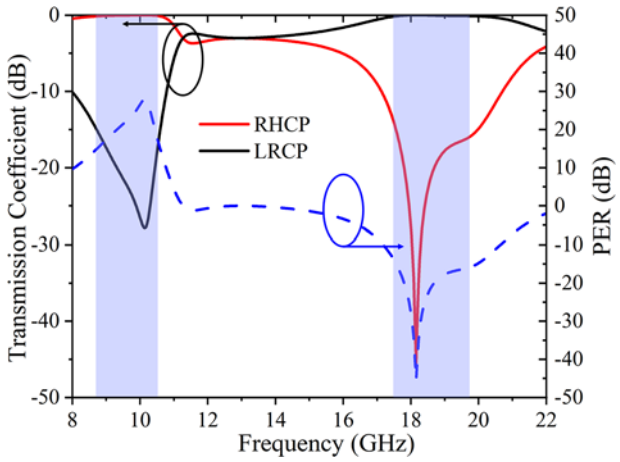

Figure 7. The linear to circular transmission responses and PERs of the proposed converter.

equal to +1 at lower band, while −1 at higher band. Such a property implies that the polarization converters based on split-ring resonators can realize the dual-band operation, and generate RHCP and LHCP waves in two frequency bands. However, the quality of AR is not sufficiently good.

Based on this, the slant dipole and square loop are used to improve the quality of circular polarization conversion. It can be seen from Fig. 6(b) that by adding the slant dipole in the middle layer, the quality of AR is considerably improved at higher band, especially higher than 17.77 GHz. Similarly, by adding the square-loop in the middle layer, the lower frequency resonance can be excited so that the curve of 3 dB AR shifts toward lower frequency, especially lower than 10.62 GHz. It should be noted that the polarization conversion performance of each case from unit cell is different due to the coupling of each subsection and its different dimensions. Table 1 presents the performance comparison of different parts of the unit cell. It can be concluded that simultaneous manipulation of slant dipole and square loop of unit cell can considerably improve the quality of 3 dB AR bandwidth, which achieve wideband linear to circular polarization conversion with orthogonal rotational modes over two operational bands.

To further investigate the circular polarization conversion performance of the proposed converter, the transmission coefficients of RHCP and LHCP waves are shown in Fig. 7. It is seen that the magnitude of RHCP and LHCP waves are greater than −0.13 dB in the frequency ranges of 8.77–10.58 and 17.59–19.88 GHz.

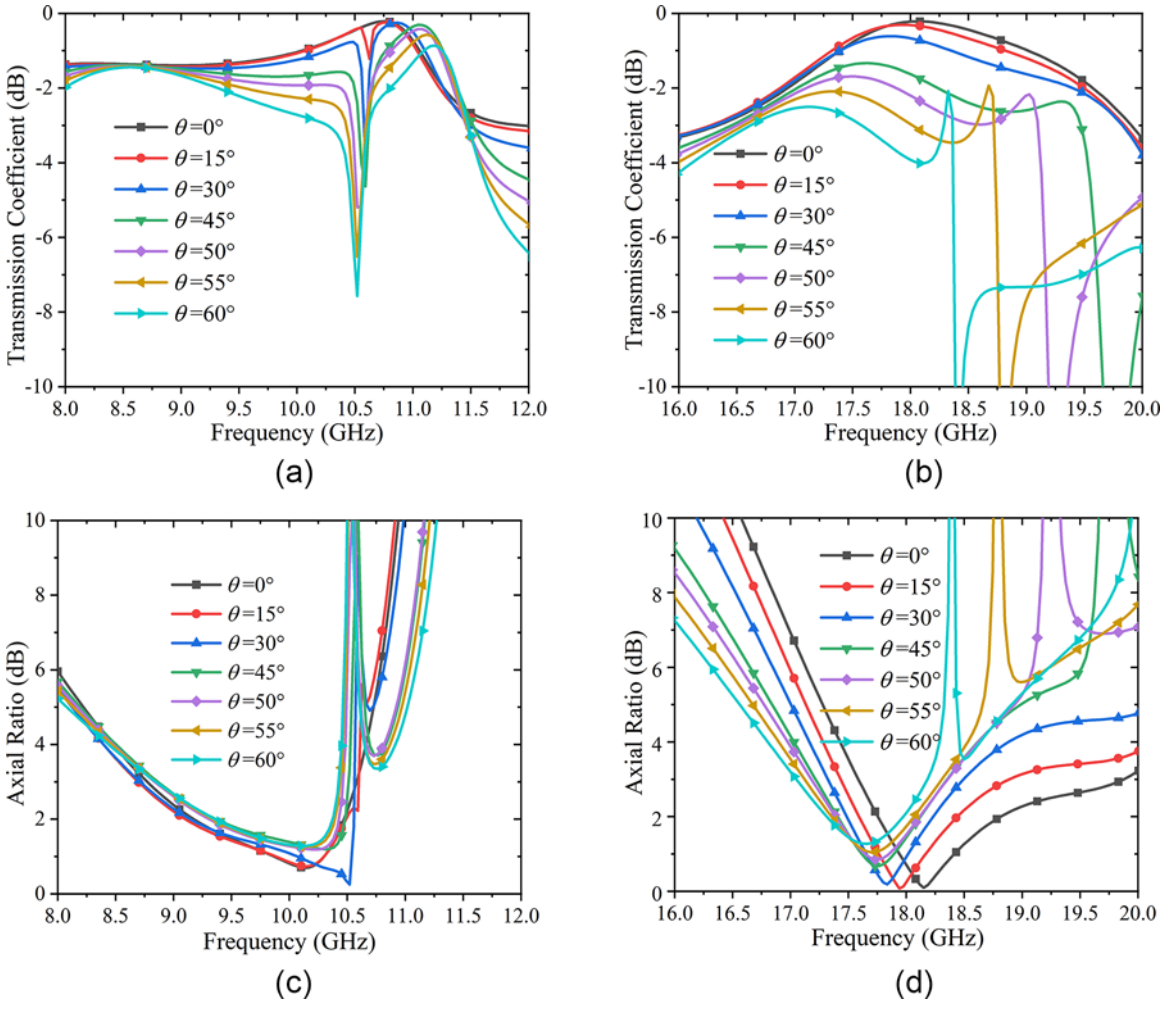

Figure 8. Simulated results at different incident angles. (a) Transmission coefficient and (c) axial ratio at lower band, (b) transmission coefficient and (d) axial ratio at higher band.

https://doi.org/10.1017/S1759078723001460 Published online by Cambridge University Press

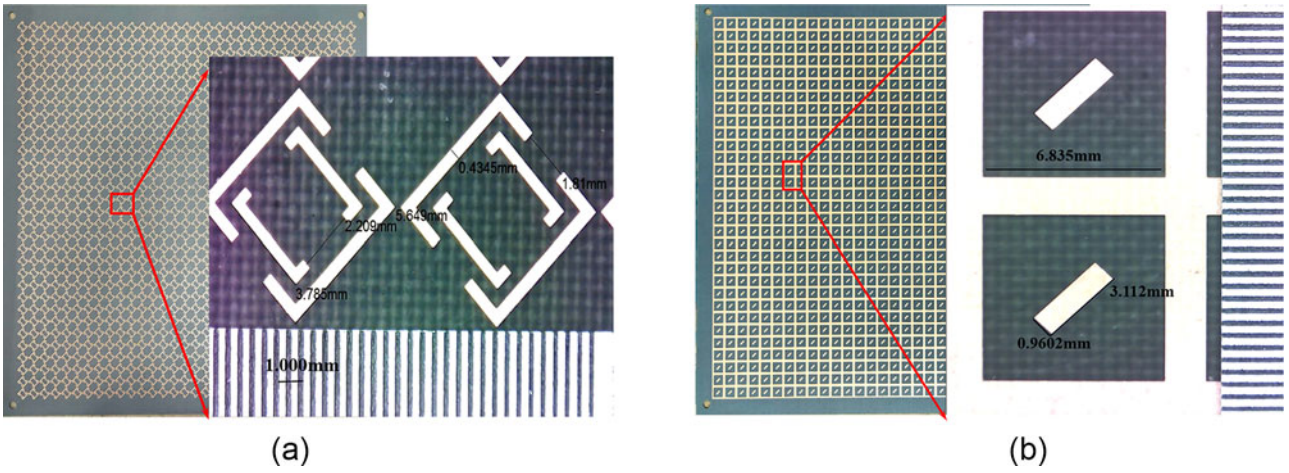

Figure 9. The fabricated sample and its unit cells photograph: (a) the first/third layer, and (b) the second layer under an industrial microscope.

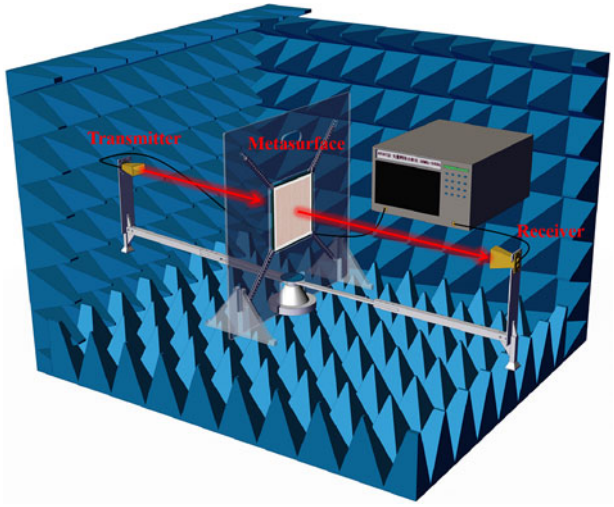

Figure 10. The illustration of the measurement setup.

Meanwhile, the polarization extinction ratios (PERs) are defined as the difference between the RHCP and LHCP waves [29]. It is found from Fig. 7 that the PERs are high in the whole operation band. They remain over 27.94 dB at 10.14 GHz and 45.49 dB at 18.15 GHz. The minimum PER nearly equals to 15.23 dB within the working bandwidth. Such a property indicates that an x-polarized incident wave can be efficiently converted into circularly polarized wave, and with high conversion efficiency. Due to the symmetrical properties of metasurface structure, this result is also valid for y-polarized incidence but with opposite polarization modes at each band.

It is also very important to assess the impact of incident angle on the polarization conversion bandwidth. Figure 8 shows the transmission coefficient and AR of the transmitted wave for different incident angles (0°, 15°, 30°, 45°, 50°, 55°, and 60°). It can be seen from Fig. 8(a) that the insertion loss of 3 dB AR bandwidth at the lower band is less than 1.7 dB when incident angle θ is below 45° while it increases to 3.5 dB when the incident angle θ up to 60°. Meanwhile, at the higher band, the insertion loss remains below 1.2 dB within 3 dB AR bandwidth when incident angle $\theta = 30°$, but it increases to 4 dB when incident angle θ up to 60°, as shown in Fig. 8(b). Besides, the angular dependence of AR in the operation band is also presented in Fig. 8(c) and (d), respectively. Apparently, the calculated AR of the proposed converter at the lower band is below 3 dB over the ranges of 0–60°. At higher band, although the AR curve moves slightly to the lower frequency, the AR still remains below 3 dB with incident angle up to 60°. This result verifies that the dual-band linear to circular polarization converter can operate at high performance with 60° angular stability.

It is noted that the miniaturization of the unit cell can provide good angular stability. For this reason, the structure utilizes square-ring as resonator to decrease side length, which saves much space for unit cell. In this design, the cell periodicity is $0.27\lambda_0$, and the thickness is $0.06\lambda_0$, where λ_0 corresponds to the wavelength of center frequency at the lower frequency band. It is evident that these dimensions from the unit cell are smaller than the operating wavelength λ_0. Thus, the unit cell shows a good miniaturization, resulting in 60° angular stability.

Experimental results

To further validate the feasibility of this design, a prototype has been fabricated using conventional printed circuit board technology, as shown in Fig. 9. It consists of 31 × 31 unit cells with an area of 257.3 × 257.3 mm^2, and is examined under an industrial microscope. It was found from Fig. 9 that the fabrication accuracy was better than 10 μm, which can provide with the good stability of bandwidth and angular incidence.

The measurement setup was illustrated in Fig. 10. The sample was surrounded by radar absorbing materials to reduce the influence of noises. Two horn antennas located at two sides of the test sample were connected to the vector network analyzer (Ceyear AV3672D) with the coaxial cables. One horn was used as the transmitting antenna, and the other as the receiving antenna. To obtain better accuracy, the sample was placed in the far-field region of the two horn antennas. For t_{xx} measurement, two horn antennas were placed along same orientation while the receiver horn antenna for t_{yx} measurements was rotated by 90°. Moreover, the transmission coefficients without the sample were measured to obtain the background. For oblique incidence measurements, the sample can be rotated along its vertical center line. In this way, both t_{xx} and t_{yx} can be derived, so that the AR can be effectively calculated.

https://doi.org/10.1017/S1759078723001460 Published online by Cambridge University Press

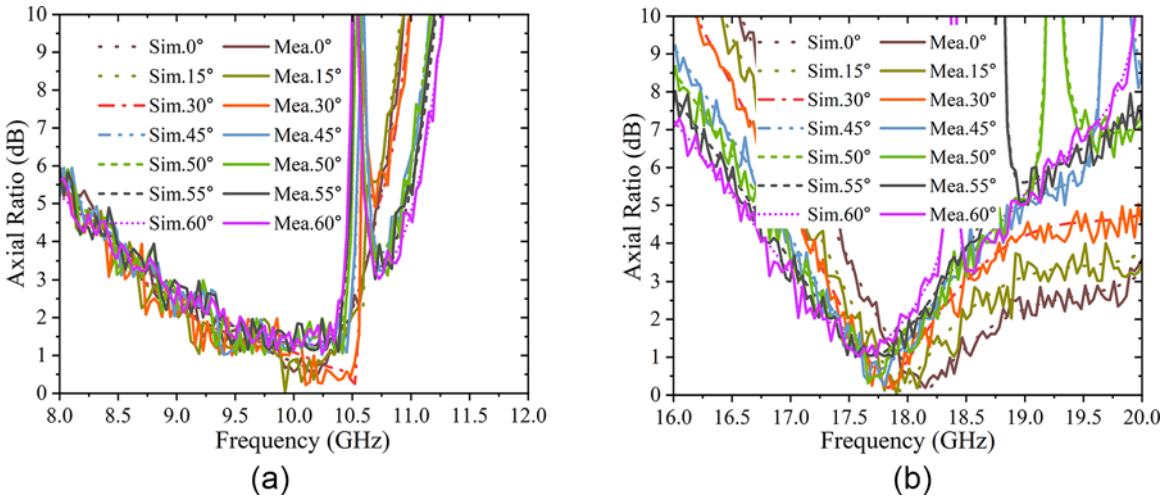

Figure 11. The comparison of simulated and measured results at different incident angles. (a) Axial ratio at lower band, (b) axial ratio at higher band.

Table 2. Performance comparison of the proposed converter with reported literature

Ref.	Center frequency (GHz)	Insertion loss (dB)	3 dB AR bandwidth (%)	Thickness	Unit cell size	Metallic layers	Angular stability (°)
[22]	10.64	<1	44.48	$0.51\lambda_0$	$0.24\lambda_0 \times 0.24\lambda_0$	>3	20
[23]	8.18	<3.2	74.01	$0.16\lambda_0$	$0.41\lambda_0 \times 0.41\lambda_0$	>3	20
[24]	10.74	<3	78.85	$0.09\lambda_0$	$0.2\lambda_0 \times 0.2\lambda_0$	2	45
[25]	19.6, 29.6	<1	7.14, 3.38	$0.52\lambda_0$	$0.63\lambda_0 \times 0.63\lambda_0$	3	–
[26]	19.95, 29.75	<1.5	2.51, 1.68	$0.56\lambda_0$	$0.47\lambda_0 \times 0.47\lambda_0$	>3	–
[27]	20.6, 29.2	<0.5, <0.4	11.65, 8.9	$0.98\lambda_0$	$0.49\lambda_0 \times 0.49\lambda_0$	>3	–
[28]	8.95, 15.81	<3.1, <3.1	36.56, 19.6	$0.09\lambda_0$	$0.30\lambda_0 \times 0.30\lambda_0$	2	–
[29]	18.5, 29	<2, <0.8	29, 12	$0.10\lambda_0$	$0.25\lambda_0 \times 0.25\lambda_0$	2	20
[30]	19.95, 29.75	<0.35, <0.79	2.51, 1.68	$0.59\lambda_0$	$0.17\lambda_0 \times 0.3\lambda_0$	>3	30
[31]	19.95, 29.75	<0.3, <0.8	2.51, 1.68	$0.07\lambda_0$	$0.35\lambda_0 \times 0.35\lambda_0$	3	45
[32]	9.35, 12.83	<0.5, <0.3	6.42, 4.29	$0.06\lambda_0$	$0.28\lambda_0 \times 0.28\lambda_0$	3	55°
[33]	7.6, 13	<3, <3	31.58, 13.85	$0.24\lambda_0$	$0.22\lambda_0 \times 0.23\lambda_0$	>3	25
This work	9.68, 18.74	<1.37, <2.9	18.71, 12.2	$0.06\lambda_0$	$0.27\lambda_0 \times 0.27\lambda_0$	3	60

It has to be mentioned that, a group of tick marks are fabricated to a rotary structure. The rotary structure with tick marks enables one to measure the angular stability conveniently. On aligning the transmitter and receiver with these tick marks, the alignment accuracy is sufficiently high, smaller than 1°.

The measured results for different incident angles are plotted in comparison with the simulated ones in Fig. 11. It can be seen that the measured results are in a good agreement with simulated ones. At x-polarized normal incidence, the converter operates with AR below 3 dB in the frequency ranges of 8.81–10.55 and 17.59–19.87 GHz, corresponding to the relative bandwidth of 18.03% and 12.17%, respectively. Moreover, for various incident angles 0–60°, the 3 dB AR bandwidth remains stable in the lower band while a slight fluctuation in the higher band. This is reasonable since all of the dimensions in the lower band are smaller than that in the higher band. However, it can be also observed that there are some slight differences between measurement and simulation in the operation band, which is very likely due to fabrication tolerances and measurement errors, such as misalignment of the horn antennas and noises in the background.

Besides, a performance comparison between the proposed converter and reported literature is presented in Table 2. It can be seen that the multilayer structures for the transmission type are frequently used to achieve wideband response [22, 23]. But there are also some designs that the bandwidth is not sufficiently wide [25–33], and performs low angular stability for oblique incidence [29, 33]. Moreover, these structures are obtained by split-ring resonators [31, 32], multilayer or superstrate layer [30, 33], resulting in the complexity of fabrication. Both types of designs can provide good angular stability [31, 32], which is reasonable since the structure is miniaturized. In the comparison, the proposed converter exhibits advantages of low profile, easy fabrication, high angular stability, and broadband response over two operational bands.

https://doi.org/10.1017/S1759078723001460 Published online by Cambridge University Press

Conclusion

In this work, a dual-band angular-stable transmissive circular polarization conversion metasurface is presented. The structure is composed of two square split-ring layers and a square loop layer nesting a slant dipole that can convert the linearly polarized incident wave into circularly polarized wave with orthogonal polarization modes in the two separate frequency bands. The simulated results show that the AR is lower than 3 dB over the frequency ranges of 8.77–10.58 and 17.59–19.88 GHz, corresponding to the relative bandwidth of 18.71% and 12.22%, respectively. Compared to other polarization converters, the proposed converter demonstrates the wideband response and 60° angular stability in the operation band. Moreover, a prototype is fabricated and measured. A good agreement was observed between measurement with simulation. Potential applications can be envisaged in dual-channel communication and other antennas such as beam scanning antenna systems.

Data availability statement. Not applicable.

Author contributions. B. Zhang did the design and simulation, C. Wang and S. Yu performed the measurement, X. Yang and Z. Fang plotted the figures, B. Zhang prepared the manuscripts, X. Liu reviewed the manuscripts and provided fundings.

Funding statement. This work is funded in part by the Natural Science Foundation of Anhui Province (2308085Y02) and the National Natural Science Foundation of China (61871003).

Competing interests. The authors report no conflict of interest.

References

1. **Saikia M, Ghosh S and Srivastava KV** (2017) Design and analysis of ultrathin polarization rotating frequency selective surface using V-shaped slots. *IEEE Antennas and Wireless Propagation Letters* **16**, 2022–2025.
2. **Baghel AK, Kulkarni SS and Nayak SK** (2019) Linear-to-cross-polarization transmission converter using ultrathin and smaller periodicity metasurface. *IEEE Antennas and Wireless Propagation Letters* **18**(7), 1433–1437.
3. **Nguyen TQH, Nguyen TKT, Nguyen TQM, Cao TN and Vu DL** (2021) Simple design of a wideband and wide-angle reflective linear polarization converter based on crescent-shaped metamaterial for Ku-band applications. *Optics Communications* **486**(1), 126773.
4. **Cui Z, Xiao Z, Chen M, Lv F and Xu Q** (2021) A transmissive linear polarization and circular polarization cross polarization converter based on all-dielectric metasurface. *Journal of Electronic Materials* **50**(7), 4207–4214.
5. **Ratni B, Lustrac A, Piau G-P and Burokur SN** (2017) Electronic control of linear-to-circular polarization conversion using a reconfigurable metasurface. *Applied Physics Letters* **111**(21), 214101.
6. **Bhattacharjee A and Dwari S** (2022) Design of an anisotropic reconfigurable reflective polarization converter for realizing circular polarization-reconfigurable antenna. *IEEE Antennas and Wireless Propagation Letters* **21**(12), 2392–2396.
7. **Xu J, Li R, Qin J, Wang S and Han T** (2018) Ultra-broadband wide-angle linear polarization converter based on H-shaped metasurface. *Optics Express* **26**(16), 20913.
8. **Long F, Yu S, Yang Z, Li X, Ding Z and Zhang Z** (2021) Broadband linear-to-circular polarization reflector using anisotropic metasurface. *International Journal of RF and Microwave Computer-Aided Engineering* **31**(7), e22697.
9. **Liao T, Zhang Z, Jiao Y, Yan Y, Chen G and Weng Z** (2021) Broadband circular polarized reflectarray based on multi-resonance unit. *International Journal of RF and Microwave Computer-Aided Engineering* **31**(6), e22618.
10. **Zhang B, Zhu C, Zhang R, Yang X, Wang Y and Liu X** (2022) Ultra-broadband angular-stable reflective linear to cross polarization converter. *Electronics* **11**(21), 3487.
11. **Mercader-Pellicer S, Goussetis G, Medero GM, Legay H, Bresciani D and Fonseca NJG** (2019) Cross-polarization reduction of linear-to-circular polarizing reflective surfaces. *IEEE Antennas and Wireless Propagation Letters* **18**(7), 1527–1531.
12. **Kundu D, Singh J, Singh D and Chakrabarty A** (2021) Design and analysis of broadband ultrathin reflective linear-to-circular polarization converter using polygon-based anisotropic-impedance surface. *IEEE Transactions on Antennas and Propagation* **69**(8), 5154–5159.
13. **Zaker R and Sadeghzadeh A** (2019) A low-profile design of polarization rotation reflective surface for wideband RCS reduction. *IEEE Antennas and Wireless Propagation Letters* **18**(9), 1794–1798.
14. **Zheng Q, Guo C, Ding J and Vandenbosch GAE** (2021) A broadband low-RCS metasurface for CP patch antennas. *IEEE Transactions on Antennas and Propagation* **69**(6), 3529–3534.
15. **Tang W, Mercader-Pellicer S, Goussetis G, Legay H and Fonseca NJG** (2017) Low-profile compact dual-band unit cell for polarizing surfaces operating in orthogonal polarizations. *IEEE Transactions on Antennas and Propagation* **65**(3), 1472–1477.
16. **Jia Y, Liu Y, Zhang W, Wang J, Wang Y, Gong S and Liao G** (2018) Ultra-wideband metasurface with linear-to-circular polarization conversion of an electromagnetic wave. *Optical Materials Express* **8**(3), 597.
17. **Salman MS, Khan MI, Tahir FA and Rmili H** (2020) Multifunctional single layer metasurface based on hexagonal split ring resonator. *IEEE Access* **8**, 28054–28063.
18. **Mao C, Yang Y, He X, Zheng J and Zhou C** (2017) Broadband reflective multi-polarization converter based on single-layer double-L-shaped metasurface. *Applied Physics A* **123**(12), 767.
19. **Doumanis E, Goussetis G, Gomez-Tornero JL, Cahill R and Fusco V** (2012) Anisotropic impedance surfaces for linear to circular polarization conversion. *IEEE Transactions on Antennas and Propagation* **60**(1), 212–219.
20. **Zheng Q, Guo C and Ding J** (2018) Wideband metasurface-based reflective polarization converter for linear-to-linear and linear-to-circular polarization conversion. *IEEE Antennas and Wireless Propagation Letters* **17**(8), 1459–1463.
21. **Pouyanfar N, Nourinia J and Ghobadi C** (2021) Multiband and multifunctional polarization converter using an asymmetric metasurface. *Scientific Reports* **11**(1), 9306.
22. **Li H, Li B and Zhu L** (2019) Wideband linear-to-circular polarizer based on orthogonally inserted slot-line structures. *IEEE Antennas and Wireless Propagation Letters* **18**(6), 1169–1173.
23. **Zhang W, Li J-Y and Xie J** (2017) A broadband circular polarizer based on cross-shaped composite frequency selective surfaces. *IEEE Transactions on Antennas and Propagation* **65**(10), 5623–5627.
24. **Zhu S, Zhao G, Yan Z, Wang Y and Zhou H** (2021) Ultra-wideband and wide-angle linear-to-circular polarizer based on single-layer dielectric substrates. *Applied Physics A* **127**(11), 821.
25. **Lundgren J, Zetterstrom O, Mesa F, Fonseca NJG and Quevedo-Teruel O** (2021) Fully metallic dual-band linear-to-circular polarizer for K/Ka-band. *IEEE Antennas and Wireless Propagation Letters* **20**(11), 2191–2195.
26. **Arnieri E, Greco F, Boccia L and Amendola G** (2020) A SIW-based polarization rotator with an application to linear-to-circular dual-band polarizers at K-/Ka-Band. *IEEE Transactions on Antennas and Propagation* **68**(5), 3730–3738.
27. **Greco F and Arnieri E** (2022) Dual-frequency linear-to-circular polarization converter for Ka-band applications. *Sensors* **22**(6), 2187.
28. **Han B, Li S, Cao X, Han J, Jidi L and Li Y** (2020) Dual-band transmissive metasurface with linear to dual-circular polarization conversion simultaneously. *AIP Advances* **10**(12), 125025.
29. **Wang HB and Cheng YJ** (2019) Single-layer dual-band linear-to-circular polarization converter with wide axial ratio bandwidth and different polarization modes. *IEEE Transactions on Antennas and Propagation* **67**(6), 4296–4301.

https://doi.org/10.1017/S1759078723001460 Published online by Cambridge University Press

30. **Zhao J, Cheng Y, Huang T and Liu P** (2021) A dual-band linear-to-circular polarization converter with robustness under oblique incidences. *Microwave and Optical Technology Letters* **63**(1), 361–366.
31. **Naseri P, Matos SA, Costa JR, Fernandes CA and Fonseca NJG** (2018) Dual-band dual-linear-to-circular polarization converter in transmission mode—application to K/Ka-band satellite communications. *IEEE Transactions on Antennas and Propagation* **66**(12), 7128–7137.
32. **Liu K, Wang G, Cai T and Li T** (2020) Dual-band transmissive circular polarization generator with high angular stability. *Optics Express* **28**(10), 14995.
33. **Zeng Q, Ren W, Zhao H, Xue Z and Li W** (2019) Dual-band transmission-type circular polariser based on frequency selective surfaces. *IET Microwaves, Antennas & Propagation* **13**(2), 216–222.

Bianmei Zhang received the master's degree in School of Computer Science and Information Engineering from Hefei University of Technology, Hefei, China, in 2015. She is currently pursuing the Ph.D. degree with the School of Physics and Electronic Information, Anhui Normal University, Wuhu, China. Her current research interests include electromagnetic metamaterials and optical communications.

Chen Wang received his master's degree of Engineering in Anhui Normal University in 2017. Currently, he works with the School of Computer and Information, Anhui Normal University. He is currently pursuing a PhD in the School of Physics and Electronic Information of Anhui Normal University. His research interests include terahertz science and technology, millimeter and sub-millimeter wave antenna measurement techniques, and electronic circuit technology.

Shuo Yu received the B.Sc. degree in electronic information engineering from the University of South China, Hengyang, China, in 2005, and the master's degree in applied mathematics from the Graduate School of China Institute of Atomic Energy, Beijing, China, in 2010. In 2017, she joined Anhui Normal University, Wuhu, China. Her research interest focuses on measurement technology and metrology science. She is holding several metrology certifications.

Xiaofan Yang received the Ph.D. degree in 2012 in electromagnetic and microwave technology at the School of Electronic Science and Engineering, University of Electronic Science and Technology of China. During the doctoral student, he joined the EHF Key Laboratory of Fundamental Science, University of Electronic Science and Technology of China. From 2011 to 2012, he has been titled as Visiting Scientist to RAL Space, Rutherford Appleton Laboratory, Science and Technology Facilities Council, at Oxford, UK. He is now with the State Key Laboratory of Complex Electromagnetic Environment Effects on Electronics and Information System, Luoyang Electronic Equipment Test Center of China. His research interests include terahertz science and technology, electromagnetic wave propagation, and millimeter and sub-millimeter wave receiver front-end.

Zhibin Fang, Senior Engineer, received the B.Sc. degree in automation major in Guangdong University of Technology in 2003, China, and Master of Science in Engineering in 2020 in School of Business Administration, South China University of Technology, China. He is now working in China Electronic Product Reliability and Environmental Testing Research Institute. His research interests include quality and reliability, automatic control, intelligent manufacturing and bioelectromagnetics.

Xiaoming Liu received the B.Sc. degree in applied physics in Nanjing University of Posts and Telecommunications in 2006, Nanjing, China, and Ph.D. degree in 2012 in electronic engineering at the School of Electronic Engineering and Computer Science, Queen Mary University of London, London, UK. In 2012, he joined the School of Electronic Engineering, Beijing University of Posts and Telecommunications. He is now with the School of Physics and Electronic Information, Anhui Normal University. His research interests include terahertz science and technology, quasi-optical techniques and systems, millimeter and sub-millimeter wave antenna measurement techniques, and bioelectromagnetics.

https://doi.org/10.1017/S1759078723001460 Published online by Cambridge University Press